LETTERS
PUBLISHED ONLINE: 4 JANUARY 2016 | DOI: 10.1038/NPHOTON.2015.252
nature photonics

Infrared spectroscopy with visible light

Dmitry A. Kalashnikov[1], Anna V. Paterova[1], Sergei P. Kulik[2] and Leonid A. Krivitsky[1]*

Spectral measurements in the infrared optical range provide unique fingerprints of materials, which are useful for material analysis, environmental sensing and health diagnostics[1]. Current infrared spectroscopy techniques require the use of optical equipment suited for operation in the infrared range, components of which face challenges of inferior performance and high cost. Here, we develop a technique that allows spectral measurements in the infrared range using visible-spectral-range components. The technique is based on nonlinear interference of infrared and visible photons, produced via spontaneous parametric down conversion[2,3]. The intensity interference pattern for a visible photon depends on the phase of an infrared photon travelling through a medium. This allows the absorption coefficient and refractive index of the medium in the infrared range to be determined from the measurements of visible photons. The technique can substitute and/or complement conventional infrared spectroscopy and refractometry techniques, as it uses well-developed components for the visible range.

Entangled photons play a crucial role in advancing many areas of quantum technologies[4–9]. They can be obtained using a variety of methods, with spontaneous parametric down conversion (SPDC) in nonlinear optical crystals being well established[10]. We consider a specific type of experiment with entangled photons, referred to as nonlinear interferometry, which is analogous to a conventional Mach–Zehnder interferometer but with the two splitting mirrors being substituted by two SPDC crystals[3]. In a nonlinear interferometer, SPDC crystals are pumped by a common laser, so that down-converted photons (signal and idler) from one crystal are injected into the second crystal. Down-converted photons from the two crystals interfere and produce an interference pattern in the frequency and spatial domains. Depending on the experimental configuration, one can observe interference either in intensity or in the second-order correlation function[11–13].

One remarkable feature of nonlinear interferometers is that the interference pattern for signal photons is determined by a total phase acquired by all three propagating photons: the signal, the idler and the pump[2,3]. This differs from conventional interferometry, where the interference pattern is defined by the phase of the signal photon. From the interference pattern of the signal photon it is possible to infer the relative phase of an idler photon. Actual detection of idler photons is not required. This scheme has found applications in imaging with undetected photons[14], interferometry below the shot noise[15], hybrid atom–light interferometers[16] and spectroscopy of Raman scattering by polaritons[17].

Here, we address the problem of the optical investigation of materials in the infrared range. A number of well-developed techniques with high sensitivity and spectral resolution are available, including transmission and Fourier-transform infrared (FTIR) spectroscopy[1]. The common requirement for such techniques is the use of infrared light sources, photodetectors and optical elements. These components often have inferior performance in terms of quantum efficiency, dark noise and loss, and are higher in cost than their visible-range counterparts. The up-conversion spectroscopy negates the need for infrared equipment, but requires the use of multiple tunable pulsed lasers[18,19]. All the above techniques are primarily designed for absorption measurement. Measurements of the refractive index require using them in conjunction with refractometers/ellipsometers. Here, a nonlinear interferometer is used for simultaneous measurements of the refractive index and absorption of a medium in the infrared range without the need for infrared equipment and sophisticated lasers. The infrared properties of the medium are inferred from the interference pattern for the signal photons in the visible range, measured with accessible optical instruments.

A nonlinear interferometer composed of two SPDC crystals pumped by a common laser is the foundation of this technique (Fig. 1). Two identical crystals with thickness L are separated by distance L_m. The crystals are set to produce signal (s) and idler (i) photons in the visible and infrared range, respectively. We assume a quasi-collinear regime of SPDC when the pump beam diameter $a \gg L_m \times \max\{\theta_s,\theta_i\}$, where $\theta_{s,i}$ is the emission angle of down-converted photons. In this case the dependence of the intensity of signal photons on the wavelength λ_s and the emission angle θ_s is given by[20]

$$I_s(\lambda_s, \theta_s) \propto \frac{1}{2}\left[\mathrm{sinc}\left(\frac{\delta}{2}\right)\right]^2 \left\{1 + \cos\left(\delta + \delta^m\right)\right\} \quad (1)$$

$$\delta(\lambda_s, \theta_s) = (k_p - k_s - k_i)L,\ \delta^m(\lambda_s, \theta_s) = (k_p^m - k_s^m - k_i^m)L_m$$

where k_j and k_j^m are the wavevectors in the SPDC crystal and gap, respectively and $j = s$, i and p for the signal, idler and pump photons, respectively. The wavevectors are given by $k_j = 2\pi n_j/\lambda_j$ and $k_j^m = 2\pi n_j^m/\lambda_j$, where n_j and n_j^m are the refractive indices of the SPDC crystal and gap, respectively. In equation (1), the first term defines the SPDC spectrum of an individual crystal, and the second term defines modulation due to interference, which depends on the phase acquired by signal, idler and pump photons in the crystals and in the medium.

When a medium with absorption at the wavelength of the idler photons is introduced into the gap, the interference pattern is given by[2,21]:

$$I_s(\lambda_s, \theta_s) \propto \frac{1}{2}\left[\mathrm{sinc}\left(\frac{\delta}{2}\right)\right]^2 \{1 + |\tau_i^m| \cos(\delta + \delta^m)\} \quad (2)$$

where τ_i^m is the amplitude transmissivity of the medium for the idler photon. We assume $|\tau_i^m| \propto \exp(-\alpha_i^m L_m)$, where $\alpha_i^m \equiv \mu_i^m/2$ is the amplitude absorption coefficient and μ_i^m is the Bouguer absorption coefficient. The visibility of the interference for signal photons, defined as $V_s = (I_{s,max} - I_{s,min})/(I_{s,max} + I_{s,min})$, vanishes as $\tau_i^m \to 0$. It can be used to calculate the absorption coefficient $\alpha_i^m = -(\ln(V_s)/L_m)$. Note that light scattering in the sample (for

[1]Data Storage Institute, Agency for Science, Technology and Research (A*STAR), Singapore 138634, Singapore. [2]Department of Physics, M.V. Lomonosov Moscow State University, Moscow 119991, Russia. *e-mail: leonid-k@dsi.a-star.edu.sg

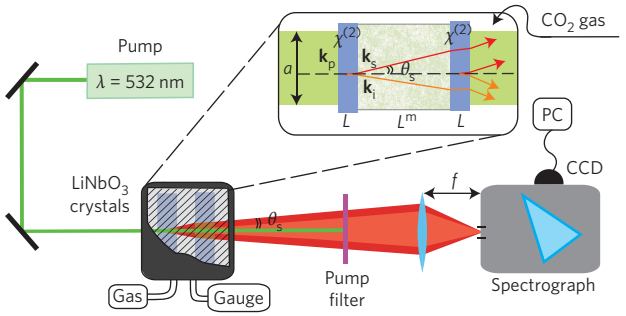

Figure 1 | Experimental set-up. A continuous-wave laser at 532 nm pumps two nonlinear crystals, where SPDC occurs. The crystals are placed in a vacuum chamber and CO_2 is injected into the chamber. The interference pattern of the SPDC from the two crystals is imaged by a lens onto a slit of a spectrograph and recorded by a charge-coupled device (CCD) camera.

example, in a bio-tissue) will contribute to degradation of the visibility (Supplementary Section 3).

From equation (2) it follows that the introduction of the medium between the crystals shifts the interference fringes due to an additional phase, proportional to n_j^m. The visibility of the fringes also decreases depending on α_i^m. Without loss of generality we assume that the medium is transparent for signal and pump photons, and that $n_{s,p}^m$ are known. Then, by fitting the measured interference pattern with equation (2), we can infer both n_i^m and α_i^m.

CO_2 gas was chosen as the medium of interest because of its importance as a greenhouse gas and also for its use in clinical breath diagnostics. CO_2 is transparent in the visible and absorbs light in the mid-infrared—the wavelength range where we demonstrate the applicability of our technique.

We studied the absorption line of CO_2 associated with an asymmetric stretching mode at a wavelength of 4.28 μm. The wavelength of an idler photon in the SPDC coincides with the centre of the absorption line of CO_2. The wavelength of the signal photon is calculated from the energy conservation for the SPDC and equals 608 nm (ref. 10).

Interference patterns in angular-wavelength coordinates for the signal photon in vacuum (20 mtorr) and at a CO_2 pressure of 7.7 torr are shown in Fig. 2a,b, respectively. The insets in each figure show the angular distribution of the intensity at a selected wavelength, indicated by the vertical dashed yellow lines. The interference fringes clearly shift and their visibility is reduced as a result of the interaction of idler photons with CO_2 (for an animation see media file in the Supplementary Information).

We first obtained the dependence of n_i^m and α_i^m on the wavelength of the idler photon. Angular cross-sections at different wavelengths of signal photons were fitted by equation (2), with n_i^m, α_i^m as the only fitting parameters (the Levenberg–Marquardt algorithm, with a confidence level of ~95%). Values of $n_{s,p}^m$ for CO_2 were taken from the literature[22] and we considered their linear dependence on the pressure. Note that the requirement of prior knowledge of $n_{s,p}^m$ can be overcome by splitting the signal and idler photons after the first crystal and then recombining them at the second crystal[14,15]. A medium can be inserted only into the path of the idler photon.

The value of α_i^m was calculated from the visibility of the pattern. The reference value of the visibility was determined from a measurement without CO_2. Experimental results at a CO_2 pressure of 10.5 torr are shown in Fig. 3a. The dependence exhibits a peak at 4.28 μm with a full-width at a half-maximum of 140 nm, which is in good agreement with calculations based on data from HITRAN (http://hitran.iao.ru), assuming the spectral resolution of our set-up.

The dependence of n_i^m on wavelength at the same pressure of CO_2 was calculated from the relative shift of the fringes from the vacuum case. The dependence is shown in Fig. 3b, and is in good agreement with theory based on the Kramers–Kronig equations, applied to the absorption data.

We also studied the dependence of α_i^m and n_i^m as a function of gas pressure at different wavelengths of the idler photon, shown in Fig. 4a,b,

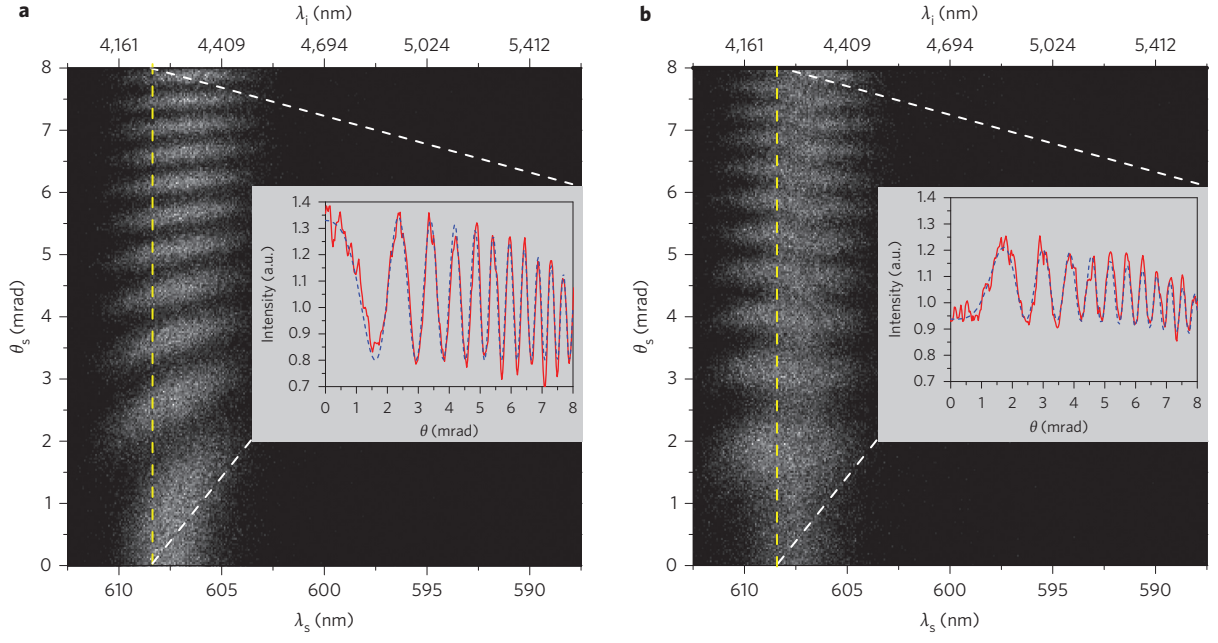

Figure 2 | Angular-wavelength intensity distribution for signal photons from two SPDC crystals. a,b, Intensity distributions obtained at pressures of 20 mtorr (vacuum) (**a**) and 7.7 torr for CO_2 gas (**b**). Absorption of idler photons by the CO_2 leads to a shift of the fringes and a decrease in their visibility. The top axes show the corresponding wavelengths of the idler photons, which are set to be close to the CO_2 resonance. Insets: angular distributions of intensity at a wavelength of signal photons of 608.5 nm (idler wavelength of 4,230 nm), denoted by yellow vertical dashed lines. In the insets, red lines show experimental data and blue dashed lines show numerical fits of the experimental data.

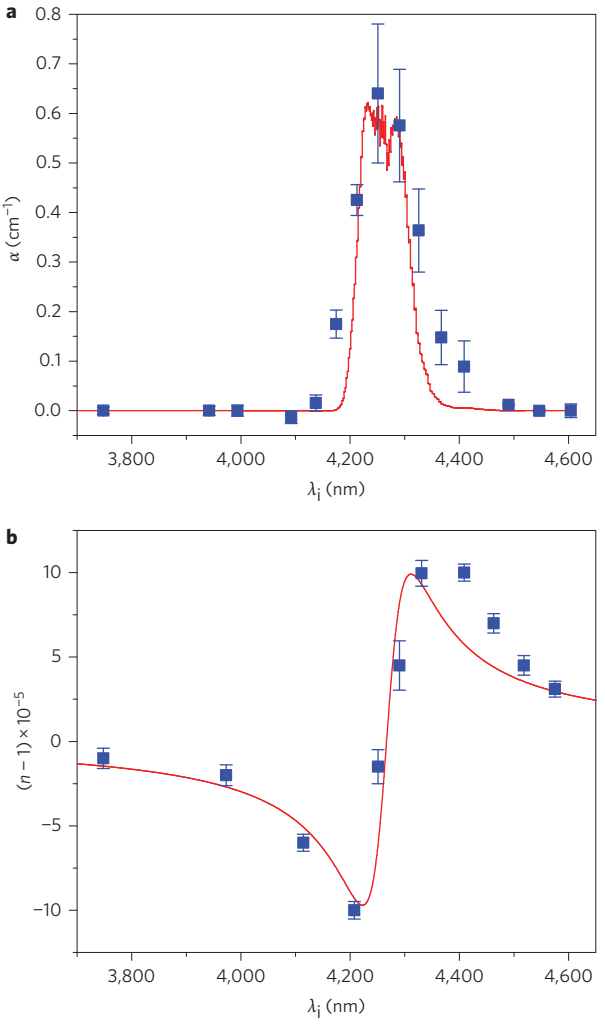

Figure 3 | Dependence on wavelength. a,b, Dependence of amplitude absorption coefficient (**a**) and refractive index (**b**) in the vicinity of the resonance for CO_2 at a pressure of 10.5 torr. Blue squares denote experimental results and red lines theoretical calculations using HITRAN data (**a**) and a Kramers–Kronig relation (**b**). Error bars indicate ±s.d. These are estimated within the fitting procedure with equation (2) assuming a normal distribution of the intensity in the interference pattern.

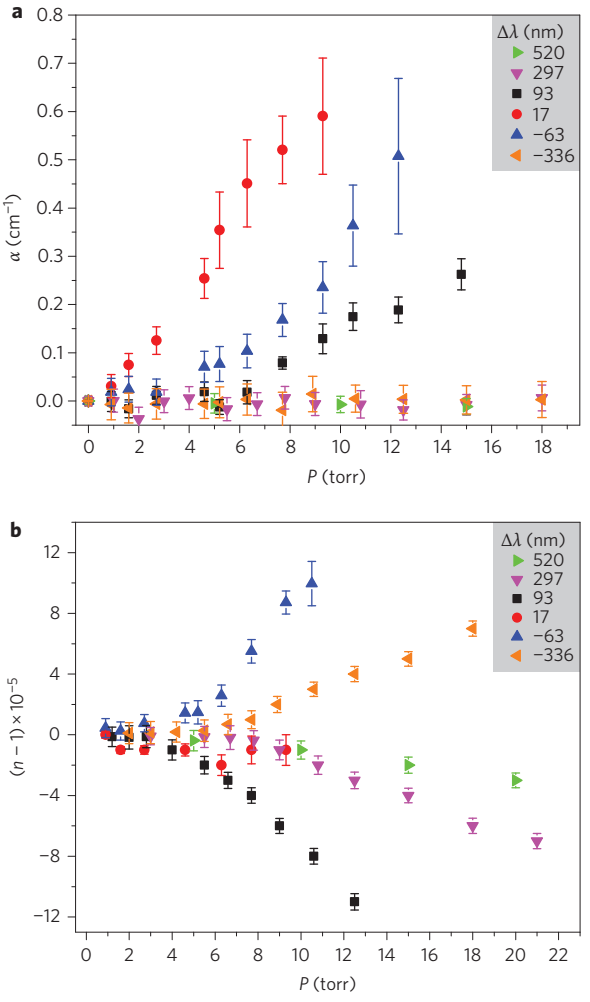

Figure 4 | Dependence on pressure. a,b, Dependence of amplitude absorption coefficient (**a**) and refractive index (**b**) on the pressure of CO_2 at various wavelengths. In the legend in grey, detuning is indicated from the central wavelength of absorption line of 4,277 nm. Error bars indicate ±s.d. These are estimated within the fitting procedure with equation (2) assuming a normal distribution of intensity in the interference pattern.

respectively. Steeper dependencies correspond to wavelengths closer to the absorption line.

The obtained dependencies exhibit nonlinearity in the vicinity of the absorption line. We explain this by different mechanisms of line broadening at different pressures[23,24]. At lower pressure, the line exhibits Doppler broadening due to the motion of molecules. At higher pressure, the line adopts a Lorentzian shape due to collision broadening. There are intermediate points between these two cases when both mechanisms play a role. However, away from the absorption line, measurements of the refractive index show a linear dependence on pressure.

In conclusion, the suggested approach allows direct measurement of the real and imaginary parts of a complex refractive index of a medium in the broadband infrared range by detecting photons in the visible range. The technique relies on nonlinear interference of frequency entangled photons, produced via SPDC. It uses a simple optical layout and accessible visible-range detector and laser. The accuracy of the technique reaches $\sim 5 \times 10^{-6}$ in the determination of the refractive index and 0.02–0.2 cm^{-1} in the determination of the absorption coefficient, accuracies that are comparable with state-of-the-art infrared methods[1]. The corresponding detection limit is 0.14 ± 0.03 mM.

Due to the broad tunability of the SPDC source, this method can be tailored to satisfy requirements for a desired operation range and spectral resolution, including the far-infrared and terahertz ranges[25,26]. The requirement to use a spectrograph can be overcome by producing narrowband, yet tunable, down-converted photons (Supplementary Section 1). Further improvement to the sensitivity is feasible by using interferometers with larger base and/or multiple-pass configurations. This approach helps to overcome some limitations of conventional infrared spectrometers and refractometers and represents a practical alternative or complementary technique for applications in materials analysis and sensing.

Methods

Methods and any associated references are available in the online version of the paper.

Received 23 June 2015; accepted 18 November 2015; published online 4 January 2016

References

1. Stuart, B. H. *Infrared Spectroscopy: Fundamentals and Applications* (Wiley, 2004).
2. Zou, X. Y., Wang, L. J. & Mandel, L. Induced coherence and indistinguishability in optical interference. *Phys. Rev. Lett.* **67,** 318–321 (1991).
3. Mandel, L. Quantum effects in one-photon and two-photon interference. *Rev. Mod. Phys.* **71,** S274–S282 (1999).
4. Gisin, N., Ribordy, G., Tittel, W. & Zbinden, H. Quantum cryptography. *Rev. Mod. Phys.* **74,** 145–195 (2002).
5. Gisin, N. & Thew, R. Quantum communication. *Nature Photon.* **1,** 165–171 (2007).
6. Knill, E., Laflamme, R. & Milburn, G. J. A scheme for efficient quantum computation with linear optics. *Nature* **409,** 46–52 (2001).
7. Ladd, T. D. *et al.* Quantum computers. *Nature* **464,** 45–53 (2010).
8. Giovannetti, V., Lloyd, S. & Maccone, L. Advances in quantum metrology. *Nature Photon.* **5,** 222–229 (2013).
9. Abadie, J. *et al.* A gravitational wave observatory operating beyond the quantum shot-noise limit. *Nature Phys.* **7,** 962–965 (2011).
10. Klyshko, D. N. *Photon and Nonlinear Optics* (Gordon & Breach Science, 1988).
11. Burlakov, A. V. *et al.* Interference effects in spontaneous two-photon parametric scattering from two macroscopic regions. *Phys. Rev. A* **56,** 3214–3225 (1997).
12. Korystov, D. Y., Kulik, S. P. & Penin, A. N. Rozhdestvenski hooks in two-photon parametric light scattering. *J. Exp. Theor. Phys. Lett.* **73,** 214–218 (2001).
13. Kulik, S. P. *et al.* Two-photon interference in the presence of absorption. *J. Exp. Theor. Phys.* **98,** 31–38 (2004).
14. Lemos, G. B. *et al.* Quantum imaging with undetected photons. *Nature* **512,** 409–412 (2014).
15. Hudelist, F. *et al.* Quantum metrology with parametric amplifier-based photon correlation interferometers. *Nature Commun.* **5,** 3049 (2014).
16. Chen, B. *et al.* Atom–light hybrid interferometer. *Phys. Rev. Lett.* **115,** 043602 (2015).
17. Polivanov, Y. N. Raman scattering of light by polariton. *Sov. Phys. Usp.* **21,** 805–831 (1978).
18. Heilweil, E. J. Ultrashort-pulse multichannel infrared spectroscopy using broadband frequency conversion in $LiIO_3$. *Opt. Lett.* **14,** 551–553 (1989).
19. Dougherty, T. P. & Heilwell, E. J. Dual-beam subpicosecond broadband infrared spectrometer. *Opt. Lett.* **19,** 129–131 (1994).
20. Klyshko, D. N. Ramsey interference in two-photon parametric scattering. *J. Exp. Theor. Phys.* **77,** 222–226 (1993).
21. Belinsky, A. V. & Klyshko, D. N. Interference of classical and non-classical light. *Phys. Lett. A* **166,** 303–307 (1992).
22. Bideau-Mehu, A., Guern, Y., Abjean, R. & Johannin-Gilles, A. Interferometric determination of the refractive index of carbon dioxide in ultraviolet region. *Opt. Commun.* **9,** 432–434 (1973).
23. Heineken, F. W. & Battaglia, A. Absorption and refraction of ammonia as a function of pressure at 6 mm wavelength. *Physica* **24,** 589–603 (1958).
24. Burch, D. E. & Williams, D. Total absorptance by nitrous oxide bands in the infrared. *Appl. Opt.* **1,** 473–482 (1962).
25. Tonouchi, M. Cutting-edge terahertz technology. *Nature Photon.* **1,** 97–105 (2007).
26. Kailash, C. J., Covert, P. A. & Hore, D. K. Phase measurement in nondegenerate three-wave mixing spectroscopy. *J. Chem. Phys.* **134,** 044712 (2011).

Acknowledgements

This work was supported by DSI core funds within the framework of the Quantum Sensors programme. The authors thank G. Vienne, R. Bakker, G. Maslennikov and D. Kupriyanov for discussions and advice on the experiment.

Author contributions

D.A.K. and L.A.K. assembled the experimental set-up and conducted the measurements. A.V.P. analysed the data and carried out numerical simulations. L.A.K. and S.P.K. conceived the idea and designed the experiment. All authors contributed to preparation of the manuscript.

Additional information

Supplementary information is available in the online version of the paper. Reprints and permissions information is available online at www.nature.com/reprints. Correspondence and requests for materials should be addressed to L.A.K.

Competing financial interests

A.V.P., D.A.K. and L.A.K. are listed as inventors for a provisional patent application on the method described in Supplementary Section 1.

Methods

Optical set-up. The pump beam from a 532 nm continuous-wave (c.w.) laser (Spectra-Physics, Millennia V) with a waist of $a = 2$ mm was sent through two identically oriented MgO:$LiNbO_3$ crystals (Castech, doped with 5% Mg, transparency range from 0.45 to 5 μm) with thickness $L = 0.5$ mm. Optical axes of the crystals were cut at 50° to the surface for type-I SPDC (extraordinary polarized pump photon and ordinary polarized signal and idler photons interaction, e → oo). The crystals were placed in a custom-made vacuum chamber (with two optical windows) at a distance of $L_m = 25$ mm from one another. Changing the orientation of the crystal optical axis allowed the frequencies of the signal and idler photons to be tuned and the CO_2 resonances at different wavelengths to be studied. The chamber was pumped down to 20 mtorr and vacuum was used as a reference medium with $n_{i,s,p} = 1$. CO_2 gas (National Oxygen, purity ≥99.99%) was fed into the vacuum chamber from a gas cylinder, and its pressure was controlled by a gauge sensor (Granville-Phillips, 275 Mini-Convectron). After passing through the crystals the pump beam was filtered by two notch filters (Semrock, NF03-532E-25). The SPDC radiation was imaged by a lens ($f = 500$ mm) onto the input slit of a spectrometer (Acton, SpectraPro 2300i). The slit of the spectrometer was positioned at the lens focal plane. At the output of the spectrometer the image of the slit, illuminated by the SPDC, was formed, providing a two-dimensional wavelength-angular distribution, which was detected by an electronically multiplied charge-coupled device camera (Andor, iXon3 888, detection range 300–1,000 nm, pixel area 13×13 μm^2). The acquisition time for the interference pattern was 10 s. Each pixel in the horizontal scale was assigned to the corresponding wavelength and each pixel in the vertical scale to the corresponding angle. Each image was saved to a PC and then processed by Mathematica and Origin software.

Dependence of refractive indices on pressure. Values of the refractive index for CO_2 in the visible range were taken from the literature[22], and we assumed that the dependence of the refractive index n on the gas pressure P followed $n(P) = 1 + ((P(n_0 - 1))/(P_0(1 + (T - T_0)/T_0)))$, where n_0 is the refractive index at atmospheric pressure P_0, T is the temperature of the gas (300 K in the present case) and $T_0 = 273$ K.